Analytical Methods

TECHNICAL NOTE

Check for updates

Effects of Dynabead type, surface chemistry, and incubation on agglomerate behavior in dual-phase microfluidic systems

Abdul Basit Zia [ID] * and Ian G. Foulds [ID]

This study investigates the agglomeration behavior of streptavidin-coated Dynabeads (M270, C1, and T1) with different sizes (2.8 μm and 1.05 μm) and surface chemistries (hydrophilic and hydrophobic) when incubated with biotinylated bovine serum albumin (bBSA) in a dual-phase microfluidic droplet system. An automated dynamic inlet microfluidic (ADIM) system generates 20-droplet trains containing 1.6 μg per mL bBSA and Dynabeads. As droplets travel through PTFE tubing at 90 μL min^{-1}, they are observed at three viewing windows corresponding to incubation times of 75 s, 125 s, and 175 s. A control experiment confirmed negligible agglomeration in bulk solution, indicating that the observed dynamics arise from the internal mixing of the droplet rather than pre-aggregation. Agglomeration dynamics are quantified using an image-analysis framework that includes a Front–Rear Intensity Difference (FRID) metric, a Band σ metric, and the standard deviation of normalized images. The results show that M270 and T1 beads exhibit rapid agglomerate growth at 125 seconds of incubation followed by redistribution toward the rear stagnation zone, whereas C1 beads display a slower, more gradual increase in signal without front-to-rear reversal. Two-way ANOVA and Tukey HSD tests demonstrated significant effects of both bead type and incubation time, as well as a strong interaction, confirming bead-specific kinetics and spatial redistribution driven by internal vortex circulation. These findings provide direct experimental evidence of vortex-induced particle transport in liquid–liquid droplets and provide insight into how Dynabead selection affects agglomeration kinetics, which is crucial for optimizing microfluidic assays and diagnostic applications.

1 Introduction

Agglutination based assays rely on detecting and quantifying agglomerates formed through the bonding of probes (streptavidin-coated particles) to targets (biotinylated proteins).[1] In microfluidic assays, droplet-based systems have proven advantageous due to their ability to minimize reagent consumption and accelerate reaction times compared to traditional methods.[2] Lab-in-tubing techniques, in particular, have demonstrated a 5–10 fold improvement in sample-to-answer time over conventional agglutination assays.[3]

In dual-phase microfluidic systems, inner vortices within droplets significantly enhance the mixing of analytes, improving reaction efficiency.[4] Kurup and Basu demonstrated that Taylor's classic model of gas–liquid plug flow extends to liquid–liquid droplets, where shear forces generate axisymmetric vortices within the droplet.[5,6] These vortices form at the front and rear of the droplet due to Laplace pressure-induced deformation. Unlike single phase microfluidic environments, where mixing is often limited, these vortices provide continuous

recirculation of suspended particles, promoting agglomerate growth over time.

Another critical factor in agglomerate formation is incubation time.[7] Studies have shown that reducing incubation time can still yield high assay sensitivity. Kennedy et al. demonstrated that antibody screening assays using the column agglutination (CAT) system allowed for a reduction to 10 minutes.[8] Castro et al. explored the biotin-streptavidin interaction, identifying optimal incubation conditions for agglutination signal strength.[3] However, these studies primarily focused on the overall measurement of agglutination rather than the spatial distribution and movement of agglomerates within droplets. In microfluidic systems, agglomerate formation is inherently dynamic, with particle motion influenced by internal vortices.[9] Since agglomerates grow continuously with mixing, a distribution of different-sized agglomerates exists within any given droplet, emphasizing the need to account for bead size variations when analyzing agglutination efficiency.

Kilili et al. compared generated clean ssDNA free of any detectable dsDNA at 20 mM NaOH, elutions from all types of Dynabeads tested (MyOne C1, M-270, M-280, and MyOne T1) to serve as a guide for other researchers that produces high-quality

School of Engineering, The University of British Columbia, Okanagan Campus, Kelowna, BC, Canada. E-mail: abdulbasit.zia@ubc.ca; Tel: +01 250 8998710

ssDNA.[10] Similarly, there is a need to investigate how Dynabeads selection affects agglomeration kinetics.

2 Material and methods

2.1 An automated dynamic inlet microfluidic (ADIM) system

Fig. 1 depicts the droplet generation and detection system. An automated dynamic inlet microfluidic (ADIM) system, previously developed,[11] is used to generate a train of droplets by modifying a 3D printer by replacing the printer head with a 3D printed nozzle. The system has a 96-well plate submerged in a reservoir of light mineral oil (M5904, Sigma-Aldrich). The streptavidin coated beads (Dynabeads M-270, C1, and T1, Invitrogen) are prepared using the trial kit from Invitrogen by Thermo Fisher Scientific in 1:1 v/v ratio with Dulbecco's Phosphate Buffered Saline (PBS). Bovine serum albumin (BSA) from Vector Laboratories (10 mg, VECTB2007) is prepared at 5000 µg mL^{-1} concentration with 1.6 µg mL^{-1} biotinylated (bBSA) while the rest is non-biotinylated (nBSA). Inclusion of non-biotinylated BSA ensures that the agglutination is non-specific bidding is not the reason for the agglomeration formation. A solution of 30 µL of premixed beads and bBSA is placed in a well of the well plate for the ADIM system to generate 20 droplets of 1 µL volume each.

In our previous experiments,[1,12] the 1.6 µg mL^{-1} concentration of M270 Dynabeads formed the agglomerates quicker and bigger in size among a wide concentration range (0.0128 µg mL^{-1} to 5000 µg mL^{-1}). The size was evaluated using image analysis and light transmittance measurements.[12] With the current pretreatment, 1.6 µg mL^{-1} concentration of M270 Dynabeads was the peak of dose curve and part of zone of equivalence.

At rest, the nozzle remains submerged in the mineral oil reservoir, maintaining continuous oil draw into the tubing. To generate a droplet, the nozzle is programmed to move vertically (along the Z-axis) into the analyte well while the vacuum pump (Gemini 2060 Dry Pump, Welch) provides a constant negative pressure. The nozzle pauses for a set delay to allow analyte uptake, then retracts to its initial position, producing a discrete analyte droplet that is immediately encapsulated by the surrounding mineral oil. The 3D printed nozzle allows the PTFE tubing to pass through and the 25-gauge needle connected at the end of the tubing. Throughout the process the droplets do not come in contact with the 3D printed nozzle.

Once generated, the droplet trains pass through PTFE tubing (0.559 mm I.D.) and are captured in video through three viewing windows. The tubing is then connected to a flow rate sensor (Sensirion SLF3S-4000B) before connecting to a vacuum pump (Gemini 2060 Dry Pump, Welch). The vacuum pump provides constant negative pressure to run the system at a 90 µL min^{-1} flow rate. The video is recorded at a resolution of 1280 × 720 pixels with a frame rate of 120 fps, a shutter speed of 1/250, and an ISO setting of 1000. The three viewing windows, spaced 30 cm apart, are positioned 45, 75 and 105 cm from the point of generation to observe incubation effects. At 90 µL min^{-1}, the viewing window gives the incubation time of $W1 = 75$ s, $W2 = 125$ s, and $W3 = 175$ s. The tubing is secured in place using a 3D-printed clear resin enclosure.

The Dynabeads Streptavidin Trial Kit includes three different streptavidin-coated Dynabeads, providing a convenient way to evaluate which Dynabeads perform best for a specific application. The kit contains 1 mL each of Dynabeads M-270 streptavidin, Dynabeads MyOne streptavidin C1, and Dynabeads MyOne streptavidin T1.

This study examines the agglutination of various types of Dynabeads with bBSA, followed by the varying incubation time and observation of the formation of agglomerates.

2.2 Analysis

Once all droplet trains are recorded in video, frames with droplets are detected using the DMV MATLAB plugin by Amar S. Basu.[13] Each droplet is captured in multiple frames as it travels across the viewing window. Then, a MATLAB script extracts the frames, crops around the droplet, resizes all images to match the smallest image size across all frames and droplets, and computes an average image for each droplet. For this dataset, images are resized to 209 by 56 pixels.

The ADIM system generates 20 droplets of 1 µL with coefficient of variance (CV) of < 10% at the rate of 6900 droplets per hour, detailed in previous publication.[11] Sparingly satellite droplets are generated due to the movement of 3D printed nozzle in and out of the analyte however, they were several magnitudes smaller than the main droplets and therefore easy to filter out during image analysis. The droplets and the spacing between them remained stable throughout the three viewing windows, providing stable set of images of each droplet for analysis.

To observe the formation of agglomerates and the effect of incubation, images of droplets at different viewing windows are analyzed using metrics previously used.[12] These metrics includes, the standard deviations of a trace line across the length of the droplet (trace σ) and the standard deviation of normalized images (normalized σ). The trace σ metric is
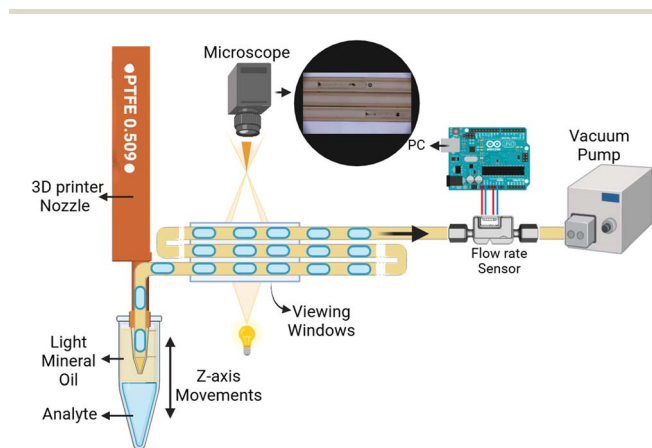

Fig. 1 Droplet generation and detection system. Droplets are generated using an automated dynamic inlet microfluidic (ADIM) system before passing through three viewing windows. Flow is under negative pressure by the vacuum pump.
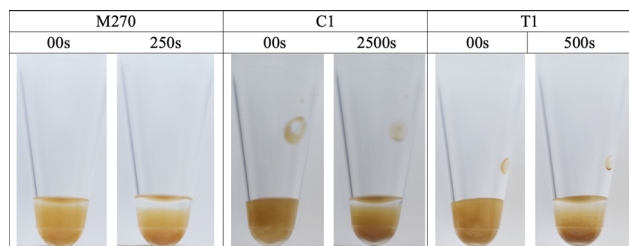
Fig. 2 Time-lapse imaging of premixed bBSA (1.6 µg mL^{-1}) and Dynabeads (M270, C1, T1) in a 1 : 1 ratio at rest in a 96-well plate. Images captured at 0 s and at extended time points (250 s for M270, 2500 s for C1, 500 s for T1) show minimal agglomerate formation and sedimentation in bulk solution without agitation. M270 beads show slight settling due to larger size (2.8 µm), while C1 and T1 (1.05 µm) remain largely suspended.

improved by calculating the standard deviation over a 30-pixel-wide horizontal band along the length of the droplet (Band σ).

2.3 Control experiment – agglutination in bulk solution

To assess whether bBSA and streptavidin-coated Dynabeads form aggregates in bulk solution prior to droplet encapsulation, time-lapse was performed on premixed samples at rest. Equal volumes (5 µL each) of bBSA (1.6 µg mL^{-1}) and Dynabeads (M270, C1, or T1) were combined in a 1 : 1 ratio in a 96-well plate, and images were captured every 10 seconds over 30 minutes. As shown in Fig. 2, minimal agglomerate formation was observed across all bead types during this period. M270 beads exhibited slight sedimentation due to their larger diameter (2.8 µm), while the smaller C1 and T1 beads (1.05 µm) remained largely suspended. The timescale for observable bulk aggregation (250–2500 s depending on bead type) substantially exceeds the 30–40 s droplet generation time, during which nozzle movement provides additional agitation that delays settling. These results confirm that the aggregation in bulk solution prior to encapsulation is negligible and does not influence the agglomeration kinetics measured within droplets.

3 Results and discussion

Table 1 shows the properties of M270, C1, and T1 Dynabeads. T1 and C1 Dynabeads have higher binding capacities to bBSA than the M-270 Dynabeads, outlined in Table 1, making them more suitable for applications that require strong capture of biomolecules. The base materials of Dynabeads M-270, C1, and

T1 influence their surface chemistry, binding efficiency, and agglomeration behavior. M-270 and C1 Dynabeads are composed of hydrophilic materials based on carboxylic acid,[14] while the T1 Dynabeads are hydrophobic and tosylactivated. The hydrophilic nature of M-270 and C1 Dynabeads enhances compatibility with polar biomolecules and provides a higher surface charge, reducing self aggregation due to electrostatic repulsion.[15,16] However, T1 Dynabeads, with a lower surface charge and hydrophobic surface, tend to aggregate more readily, leading to faster and potentially larger agglomerate formation. Generally, M-270 and C1 Dynabeads are ideal for controlled, gradual agglomeration, while T1 Dynabeads are better suited for rapid, large agglomerate formation, particularly when working with hydrophobic targets. Choosing the appropriate bead type depends on the desired agglomeration behavior and stability required for a specific assay.[17]

3.1 Results

3.1.1 Mean trace line. Fig. 3 presents the mean pixel intensity along a horizontal trace line through the center of all droplets at a 1.6 µg mL^{-1} concentration for M270, C1, and T1 Dynabeads respectively, through the three viewing windows (W1, W2, and W3). The peaks at the beginning and end correspond to the droplet edges. The viewing window corresponds to the incubation time of $W1 = 75$ s, $W2 = 125$ s, and $W3 = 175$ s. The start of the droplet is at zero pixel and the droplet ends at the 209th pixel. The non-uniform intensity profile along the droplet length originates from axial concentration gradients caused by recirculating vortices within the plug.[5,6] As incubation progresses, these vortices promote bead transport toward the rear stagnation zone, resulting in the observed asymmetry. To quantify changes in intensity from the front to the back of the droplet, a new metric called Front–Rear Intensity Difference (FRID) was computed for each droplet. For every droplet, the mean intensity of pixels in the front half (1st–104th pixel) and rear half (105th–209th) is computed, and their difference (front–rear) is denoted FRID. A positive FRID indicates stronger agglomeration in the front, while a negative value indicates stronger agglomeration in the rear. The FRID values were used in a two-way ANOVA (Bead Type × Incubation Time) followed by Tukey HSD comparisons.

Fig. 3a shows the mean traces for M270 Dynabeads. At window 1, agglomerates are primarily observed in the front half of the droplet. As the droplet progresses through subsequent viewing windows, the agglomerate size in the front half

Table 1 Main properties of Dynabeads M-270, C1, and T1

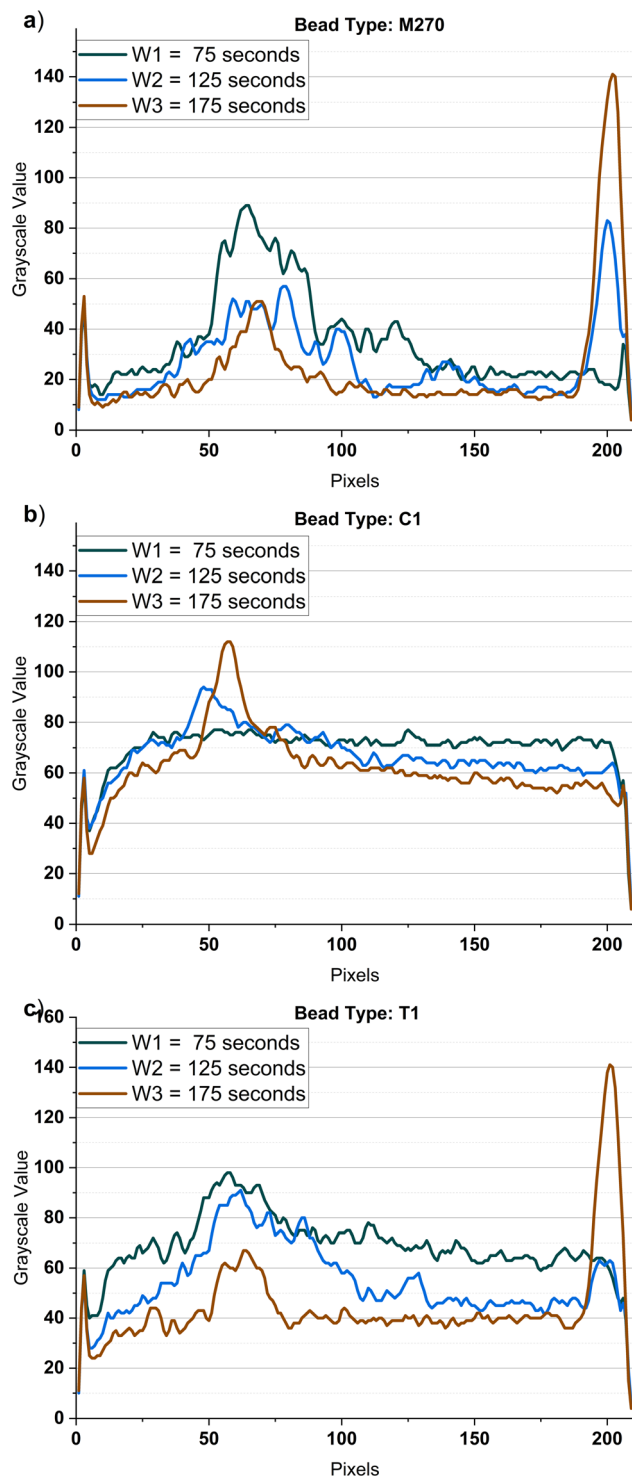| Property	M-270	C1	T1
Surface type	Hydrophilic	Hydrophilic	Hydrophobic
Base material	Carboxylic acid	Carboxylic acid	Tosylactivated
Diameter (µm)	2.8	1.05	1.05
Biotinylated Ig binding (µg mg^{-1})	5–10	15–20	Up to 20
Surface charge (mV)	High (−50)	Medium (−35)	Low (−10)
Blocking protein	None	None	BSA
Iron content (ferrites)	14% (20%)	26% (37%)	26% (37%)

Fig. 3 Mean of traces along the length of the droplet for different bead types (a) M270, (b) C1, and (c) T1 at three incubation times: $W1 = 75$ seconds, $W2 = 125$ seconds, and $W3 = 175$ seconds.

decreases, while they begin to settle toward the rear. By window 3, a distinct peak forms at the back of the droplet, indicating accumulation in a stagnation zone formed at the back identified by Kurup and Basu.[5] This visual observation is confirmed quantitatively by FRID. The mean FRID for M270 decreases

from a $+19.2$ value at 75 s, to $+7.8$ at 125 s, and then to -4.0 at 175 s. These values represent the mean of all droplets' FRID values. Tukey HSD shows no significant difference between M270 and other bead types when averaged across all incubation times ($p = 0.427$), but the bead $\times$ time interaction is highly significant ($p < 0.001$, $F_{(4,198)} = 30.34$, $\eta^2 = 0.33$). This confirms that M270's spatial distribution changes strongly with incubation time. The reversal from positive to negative FRID demonstrates migration from the front toward the rear stagnation zone as incubation increases.

Fig. 3b shows the mean traces for C1 Dynabeads. Ignoring the peaks at the beginning and the end, the mean trace displays evenly spread Dynabeads for window 1. The second window shows some peak at the front half of the droplet that gets more prominent by the third window. The C1 Dynabeads transitions from slightly rear-biased at 75 s of incubation (FRID = -0.5) to increasingly front-biased at 125 s and 175 s of incubation (FRID = $+9.68$ and $+11.6$ respectively). Unlike M270 and T1, the trend does not reverse from front to rear, instead stabilizes as front biased. The slight negative value of FRID value at 75 s of incubation might be due to peaks at the edges of the droplet. ANOVA shows that incubation time is significant ($p < 0.001$), and Tukey HSD reveals that C1 at 75 s is significantly different from C1 at both 125 s and 175 s. Thus, C1 shows time-dependent increase in front accumulation, but no front-to-back reversal. The C1 Dynabeads has a lower sedimentation rate compared to M270, according to datasheet,[17] hence we do not see agglomerates accumulation at the back of the droplet.

Fig. 3c shows the mean traces for T1 Dynabeads. The mean trace for T1 shows better agglomerate formation as compared to C1. In window 1, the front half of the droplet shows a more prominent peak compared to C1 in window 1. The magnitude of the gray-scale value of the peak is higher than M270 Dynabead due to faster kinetic,[17] although it drops for window 2 and is lowest for window 3 in the front half of the droplet. This is due to the accumulation of agglomerates at the back of the droplet. T1 Dynabeads exhibit FRID values of $+8.79$ (75 s), $+13.71$ (125 s), and -5.45 (175 s), showing a reversal from front to rear accumulation at extended incubation times. The sign change indicates a strong migration toward the rear at late incubation. This front-to-rear shift matches the behavior of M270, although the timing differs. Together, the FRID data and the ANOVA interaction effect ($F_{(4,198)} = 30.34$, $p < 0.001$) demonstrate that the spatial distribution of agglomerates is both incubation-time dependent and bead-specific.

3.1.2 Trace Line's σ and Band's σ. The previous section shows how the mean trace line along the droplet length allows us to learn about the general behavior of agglomerates of different types of Dynabeads. The standard deviation of the trace line has been used in the past to evaluate agglutination[12] of M270 Dynabeads with bBSA. Instead of a line along the droplet length, a band of 30 pixels wide (covering $\approx 50\%$ of droplet height) is chosen and its standard deviation is plotted as BandTrace in Fig. 4. For the three types of beads at different concentrations. To evaluate which metric better captures agglomeration changes with incubation time, both metrics were compared using ANOVA, effect size (Cohen's d), signal-to-noise
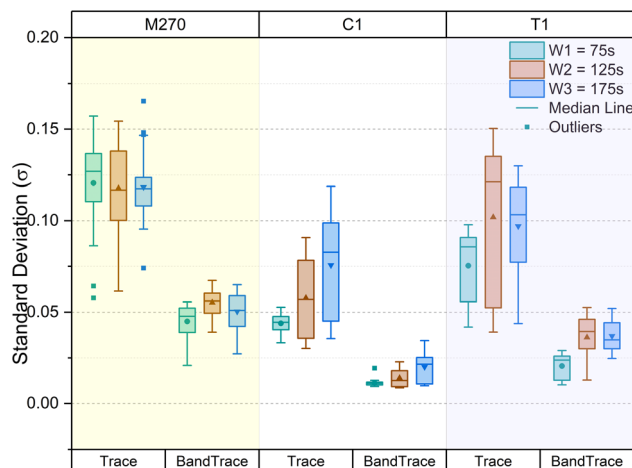
Fig. 4 Standard deviation of traces along the length of the droplet in comparison with a standard deviation of 30 pixels wide horizontal band across droplet for different bead types (M270, C1, T1) at three incubation times: ($W1 = 75$ seconds, $W2 = 125$ seconds, and $W2 = 175$ seconds).

ratio, and coefficient of variation. The results demonstrate that the Band σ metric consistently outperforms the Trace σ metric for all bead types.

For M270 Dynabeads, the trace σ values remain nearly constant across all viewing windows. This indicates that the clusters are homogenous, and the size does not change significantly over time. This observation is confirmed statistically as Trace σ shows no significant difference across incubation times ($p = 0.94$), whereas Band σ shows a highly significant difference ($p = 0.0005$) with a much larger F-statistic (8.45 compared to 0.06 for Trace). Furthermore, the effect size for the transition between 75 and 125 s increases from 0.09 (Trace) to 1.27 (Band), indicating that Band σ provides far stronger discrimination between time points.

For C1 Dynabeads, the overall mean of trace σ and band σ both show an increase across the viewing window for both cases. For this bead type, Band σ demonstrates slightly stronger separation between incubation times ($F = 15.3$ vs. $F = 15.0$ for Trace), though with comparable or slightly higher variability (mean CV of Trace $\sigma = 28.09$).

For T1 Dynabeads, both the Trace and Band σ show an increase across the viewing windows with a higher intensity for trace σ. However, Band σ provides a much clearer separation of incubation times. Band σ achieves an F-statistic of 19.3 ($p < 0.001$), compared with only 4.34 for Trace σ. The effect size between 75 and 125 s increases from 0.82 (Trace) to 1.58 (Band). This confirms that Band σ better captures the strong hydrophobic-driven agglomeration behavior of T1 beads by reducing noise and enhancing temporal contrast.

Across all bead types, Band σ generally provides stronger or comparable statistical separation and effect sizes compared to Trace σ, and for M270 and T1 it also offers lower variability. For C1, Band σ improves separation at longer incubation times (125 s to 175 s), but this comes with slightly higher variability.

3.1.3 Standard deviation (σ) of normalized images. In previously reported research,[12] it is established that the

standard deviation of agglutinated droplets is significantly different from non-agglutinated droplets. Therefore, Fig. 5 shows the standard deviation of normalized images for each droplet for different bead types at different incubation times.

In general, the mean value of all droplets increases in Fig. 5 with an increase in incubation time (viewing windows). For M270 Dynabeads (2.8 μm, −50 mV surface charge), the high negative zeta potential provides strong electrostatic stabilization through double-layer repulsion, consistent with DLVO theory.[18,19] The signal peak at 125 s followed by decline at 175 s reflects steric saturation, as biotin-streptavidin complexes accumulate on the bead surface, polymeric chains create excluded volume barriers that prevent additional protein approach.[20,21]

For T1 Dynabeads (1.05 μm, −10 mV, hydrophobic surface), weak electrostatic repulsion allows van der Waals attractive forces and hydrophobic interactions to dominate. The hydrophobic effect drives entropically favorable self-association as beads minimize unfavorable water-hydrophobic surface contact,[22] competing with productive biotin binding at longer incubation times.

C1 Dynabeads show gradual, sustained signal increase due to balanced colloidal forces with an intermediate surface charge (−35 mV) that provides moderate electrostatic stabilization, while smaller size (1.05 μm) reduces gravitational settling. Moreover, the Tween 20 surfactant provides additional steric stabilization through adsorbed polymer layers.[17]

Two-way ANOVA is performed to statistically evaluate the effects of bead type and incubation time on the normalized-image standard deviation. Both bead type and incubation time were found to be highly significant ($p < 0.001$ for both factors), and the interaction between them is also statistically significant ($p < 0.001$). This confirms that the extent of agglomeration depends not only on incubation time but also on the specific surface chemistry and physical properties of each bead type. *Post hoc* Tukey HSD comparisons further validated the trends observed visually in Fig. 5. For M270 and T1 Dynabeads, the normalized image standard deviation increases significantly from 75 s to 125 s and then shows a slight but
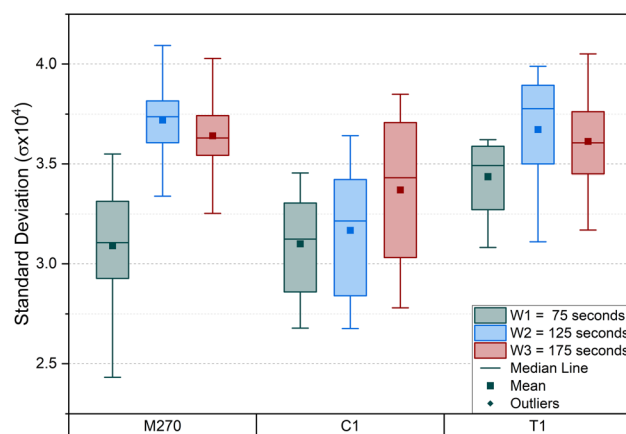

Fig. 5 Standard deviation of normalized images of the droplet for different bead types (M270, C1, T1) at three incubation times: $W1 = 75$ seconds, $W2 = 125$ seconds, and $W3 = 175$ seconds.

statistically significant reduction by 175 s of incubation. This supports the interpretation that these beads experience rapid biotin–streptavidin binding followed by saturation and redistribution of larger aggregates. For C1 Dynabeads, the increase in standard deviation from 75 seconds to 175 seconds was statistically significant but more gradual, consistent with smaller bead size, lower surface charge, and surfactant-mediated interactions.

3.2 Discussion and future works

While the current analysis provides a comparative evaluation of M270, C1, and T1 Dynabeads, further improvements can be achieved by employing more robust data analysis methodologies. A more comprehensive comparison between these beads requires additional experiments with a broader range of biotinylated BSA (bBSA) concentrations to better understand binding efficiency and saturation kinetics.

Kilili et al.[10] compared M-270, M-280, MyOne C1, and MyOne T1 Dynabeads for DNA purification quality, identifying differences in performance based on bead properties. Our study extends this comparative framework to agglomeration kinetics in microfluidic droplets, revealing how the same surface chemistry differences affect biotin-binding dynamics over time. While Kilili et al. focused on endpoint purity, we demonstrate temporal evolution of agglomerate formation.

Kurup and Basu[5,6] established that Taylor plug-flow generates axisymmetric recirculation patterns within droplets, with stagnation zones at the front and rear due to Laplace pressure-induced deformation. Building on this fluid dynamics framework, our observations reveal that M270 and T1 agglomerates preferentially accumulate at the rear stagnation zone (Fig. 2a and c), with redistribution from front to rear occurring over increasing incubation time. Our study provides direct experimental evidence of vortex-induced particle accumulation, complementing the numerical simulations of Maleki et al.[4] and corroborating the co-rotating vortex models described by Kurup and Basu. This spatial segregation of biotin-streptavidin bead agglomerates within vortex patterns has not been previously characterized for bead-based agglutination assays in dual-phase microfluidic systems and has implications for assay design where optical detection position matters.

Additionally, the current study utilizes a 1 : 1 ratio of beads to BSA, but exploring different ratios would provide deeper insights into the dynamics of agglomerate formation. Testing lower bead-to-bBSA ratios, for example, could be particularly valuable as it may allow for particle image velocimetry (PIV) analysis to visualize and characterize vortex patterns generated inside the droplets. This approach would enhance our understanding of the internal flow dynamics and potential interactions between the Dynabeads within microfluidic droplets.

By integrating these expanded experimental conditions with advanced data analysis techniques, future studies can more fully characterize binding dynamics, agglomerate behavior, and microfluidic flow patterns, improving the applicability of Dynabeads in various biotechnological and analytical applications.

4 Conclusion

This study examined the impact of Dynabead type, surface chemistry, and incubation time on agglomerate formation within microfluidic droplets. The analysis demonstrated that bead size, surface charge, and hydrophilicity/hydrophobicity significantly influence the agglomeration behavior and spatial distribution within droplets over time.

Among the tested Dynabeads, M270 and T1 exhibited a rapid increase in signal up to 125 s of incubation, followed by a decline at 175 s, likely due to steric hindrance (M270) and hydrophobic self-association (T1). In contrast, C1 Dynabeads displayed a more gradual increase in signal, suggesting a slower but sustained agglomeration process. The findings highlight the importance of selecting appropriate bead types for specific applications, particularly in assays where controlled vs. rapid agglomeration is critical.

Additionally, the results emphasize the role of internal vortex-driven mixing in agglomerate distribution within droplets as agglomerates accumulate in stagnation zones of the droplet.

Author contributions

I. G. F. (Ian G. Foulds) and A. B. Z. (Abdul Basit Zia) worked on the original conceptualization. A. B. Z. designed, performed the experiments, analyzed data, and wrote the manuscript. I. G. F. reviewed, proofread, and approved the manuscript. The work was done under the supervision of I. G. F.

Conflicts of interest

There are no conflicts to declare.

Data availability

The dataset supporting the findings of this study, titled "Borealis Dataset: SP3/H6TIFE", is publicly available on the Borealis repository. It includes image data on the effect of flow rate, tubing, and incubation for DynaBeads Streptavidin with biotinylated BSA droplets in dual-phase lab-in-tubing microfluidics. The dataset can be accessed at https://doi.org/10.5683/SP3/H6TIFE.

Acknowledgements

Notes and references

1 J. Farrell, A. B. Zia and I. G. Foulds, *IEEE Sens. Lett.*, 2023, **7**, 1–4.

2 B. Teste, A. Ali-Cherif, J. L. Viovy and L. Malaquin, *Lab Chip*, 2013, **13**, 2344–2349.

3 D. Castro, D. Conchouso, R. Kodzius, A. Arevalo and I. G. Foulds, *Genes*, 2018, **9**, 281.

4 M. A. Maleki, M. Soltani, N. Kashaninejad and N.-T. Nguyen, *Phys. Fluids*, 2019, **31**, 032001.

5 G. K. Kurup and A. S. Basu, *Annual International Conference of the IEEE Engineering in Medicine and Biology Society*, 2011, pp. 4034–4037.

6 G. K. Kurup and A. S. Basu, *Biomicrofluidics*, 2012, **6**, 1–11.

7 S. Lee and H. Kim, *Bull. Korean Chem. Soc.*, 2021, **42**, 80–86.

8 G. Kenneday, H. J. Chih, S. Finch and P. Ellery, *Transfus. Med.*, 2023, **33**, 379–389.

9 A. Mudugamuwa, U. Roshan, S. Hettiarachchi, H. Cha, H. Musharaf, X. Kang, Q. T. Trinh, H. M. Xia, N.-T. Nguyen and J. Zhang, *Small*, 2024, **20**, 2404685.

10 G. K. Kilili, L. Tilton and C. M. Karbiwnyk, *BioTechniques*, 2016, **61**, 114–116.

11 A. B. Zia, J. Farrell and I. G. Foulds, *Lab Chip*, 2024, **24**, 3015–3026.

12 A. B. Zia, J. Farrell and I. G. Foulds, *Integrating Image Analysis and Low-Cost Optical Transmittance for Quantification of Agglutination in a Dual-Phase Automated Dynamic Inlet Microfluidics System*, 2024, Advance Copy, DOI: 10.2139/ssrn.4940936.

13 A. S. Basu, *Lab Chip*, 2013, **13**, 1892–1901.

14 T. F. Scientific, *Dynabeads™ M-270 Carboxylic Acid Datasheet*, 2023.

15 T. F. Scientific, *Dynabeads™ M-270 Streptavidin User Guide*, 2023.

16 T. F. Scientific, *Dynabeads™ M-270 Streptavidin Product Page*, 2023.

17 Thermo Fisher Scientific, Dynabeads Streptavidin Manual and Automated Protocols, 2023, https://assets.thermofisher.com/TFS-Assets/LSG/brochures/dynabeads-streptavidin-manual-automated-brochure.pdf, Accessed: 2025-02-03.

18 E. J. W. Verwey and J. T. G. Overbeek, *Theory of the Stability of Lyophobic Colloids*, Elsevier, Amsterdam, 1948.

19 H. Ohshima, *Electrical Phenomena at Interfaces and Biointerfaces*, John Wiley & Sons, 2014, pp. 147–163.

20 G. Fritz, V. Schädler, N. Willenbacher and N. J. Wagner, *Langmuir*, 2002, **18**, 6381–6390.

21 D. H. Napper, *Polymeric Stabilization of Colloidal Dispersions*, Academic Press, London, 1983.

22 M. Borkovec, I. Szilagyi, I. Popa, M. Finessi, P. Sinha, P. Maroni and G. Papastavrou, *Adv. Colloid Interface Sci.*, 2012, **179–182**, 85–98.